

Universidade Federal da Bahia
IME – PGCOMP
MATE06 - TÓPICOS EM COMPUTAÇÃO VISUAL I
Seminário
Professor: Antônio L. Apolinário Jr.
Aluno: Fernando Ferraz Ribeiro

Conceitos:

Tessellation

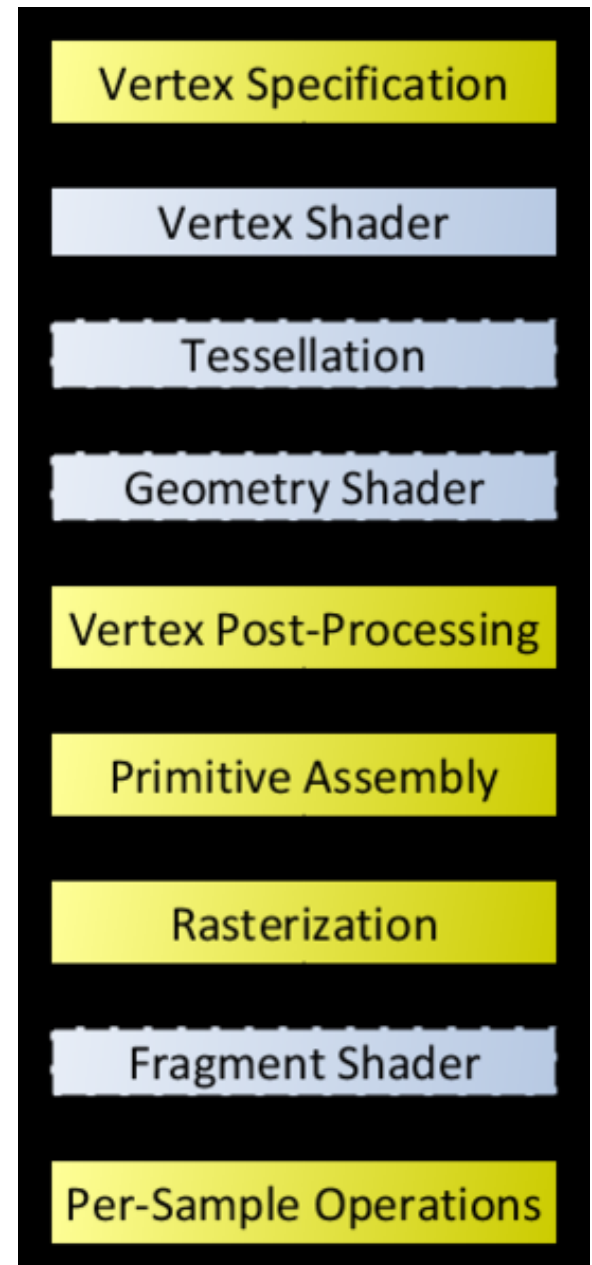
Bezier

Spline

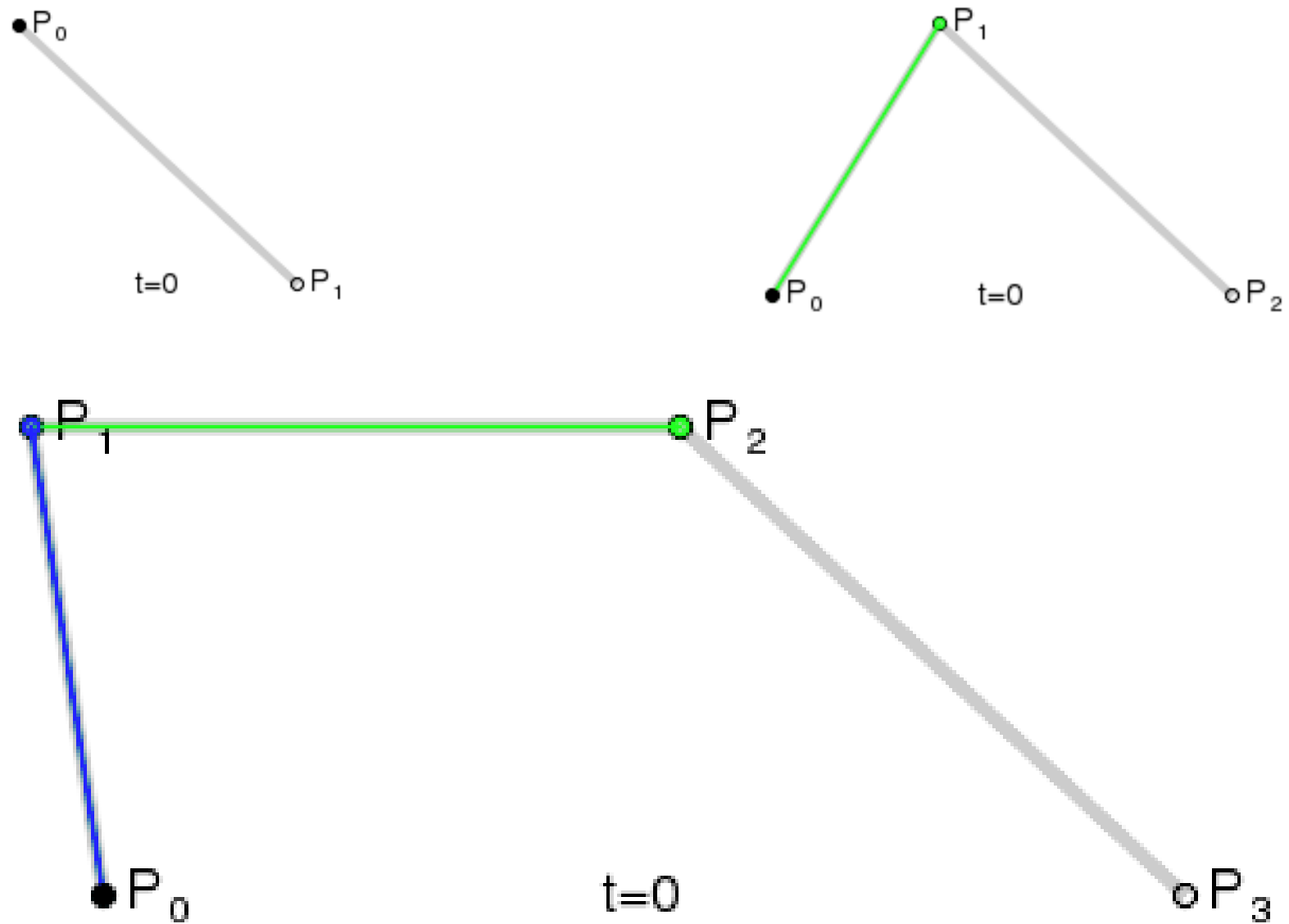
Nurbs

Tessellation

Tessellation é a etapa do processamento dos vértices do pipeline gráfico Opengl que transforma primitivas do modelo em primitivas menores.



Bezier



ARTIGO 1:

Phong Tessellation

Tamy Boubekeur Marc Alexa

TU Berlin

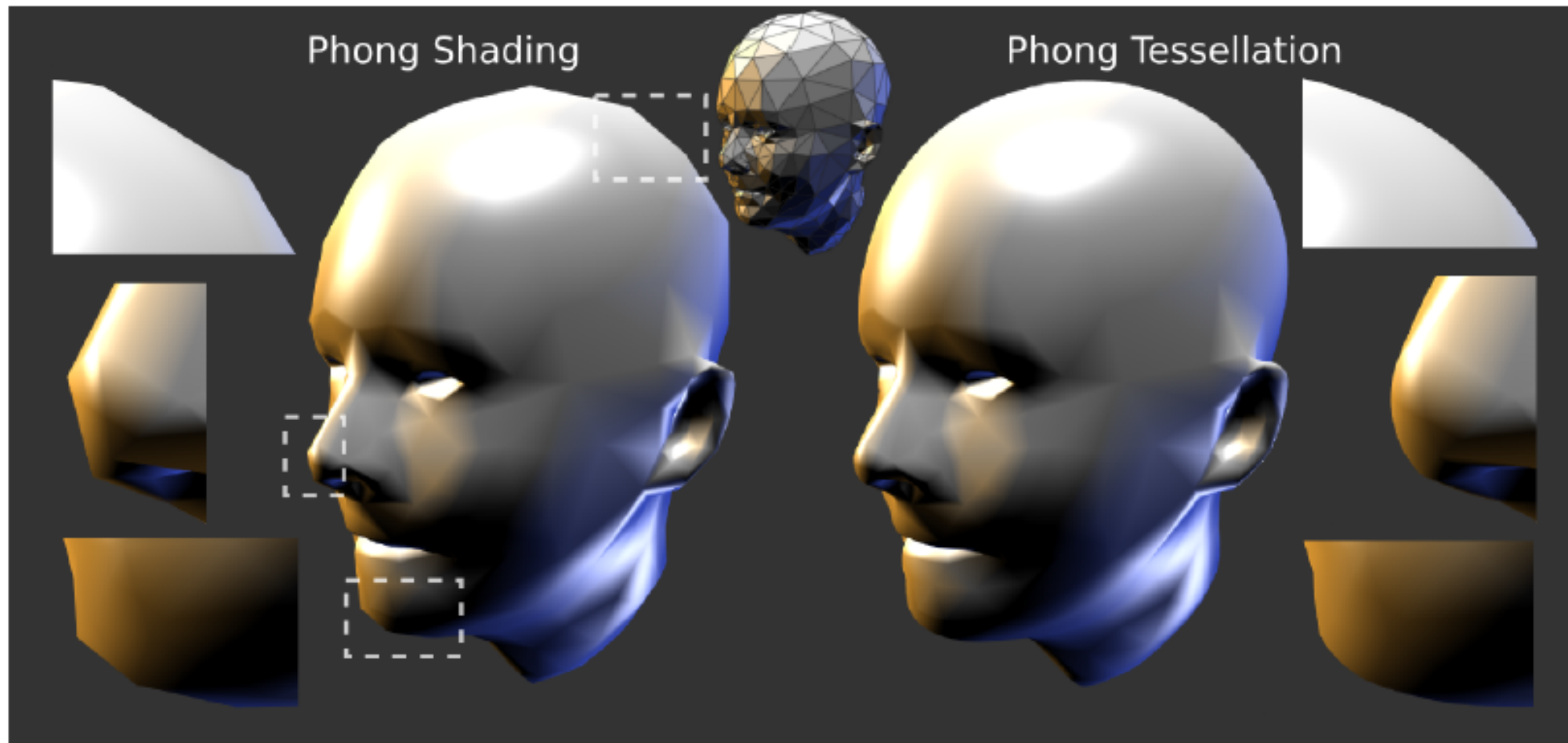


Figure 1: *Phong Tessellation completes Phong Shading.*

Gouraud - Phong

Gouraud $\mathbf{p}(u, v) = (u, v, w)(\mathbf{p}_i, \mathbf{p}_j, \mathbf{p}_k)^T$ (1)

Phong $\mathbf{n}'(u, v) = (u, v, w)(\mathbf{n}_i, \mathbf{n}_j, \mathbf{n}_k)^T, \quad \mathbf{n}(u, v) = \mathbf{n}' / \|\mathbf{n}'\|$ (2)

Phong Tessellation

1. Calcular a interpolação linear.
2. Projetar o ponto interpolado nos 3 planos tangentes a cada vértice que contenham as normais dos vértices.
3. Calcular a interpolação linear em relação ao triângulo gerado pelos pontos projetados.

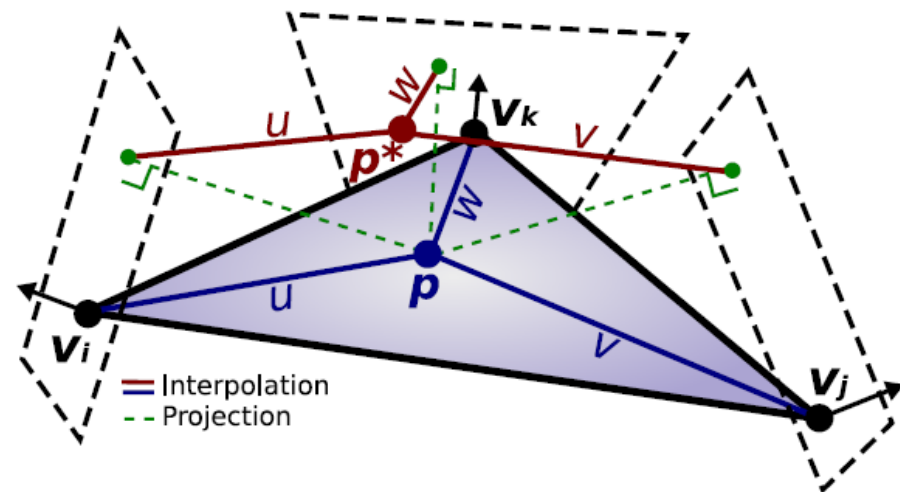


Figure 3: Phong Tessellation principle. Instead of interpolating normals as in Phong Shading, we interpolate projection onto vertices tangent plane to define a curve geometry for each triangle.

Phong Tessellation

$$\pi_i(\mathbf{q}) = \mathbf{q} - ((\mathbf{q} - \mathbf{p}_i)^T \mathbf{n}_i) \mathbf{n}_i$$

$$\mathbf{p}^*(u, v) = (u, v, w) \begin{pmatrix} \pi_i(\mathbf{p}(u, v)) \\ \pi_j(\mathbf{p}(u, v)) \\ \pi_k(\mathbf{p}(u, v)) \end{pmatrix}$$



Figure 5: Convex, saddle and concave normals configuration.

Fator Alfa

$$\mathbf{p}^*_{\alpha}(u, v) = (1 - \alpha)\mathbf{p}(u, v) + \alpha(u, v, w) \begin{pmatrix} \pi_i(\mathbf{p}(u, v)) \\ \pi_j(\mathbf{p}(u, v)) \\ \pi_k(\mathbf{p}(u, v)) \end{pmatrix} \quad (4)$$

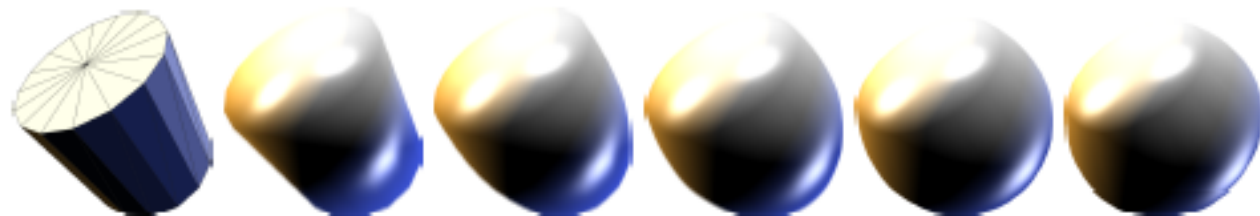


Figure 4: Coarse mesh, followed by various Phong Tessellations with α equal to 0, 1/4, 1/2, 3/4 and 1.

Propriedades

$$\begin{aligned}\mathbf{p}^*(u, v) = & u^2 \mathbf{p}_i + v^2 \mathbf{p}_j + w^2 \mathbf{p}_k + uv (\pi_i(\mathbf{p}_j) + \pi_j(\mathbf{p}_i)) + \\ & vw (\pi_j(\mathbf{p}_k) + \pi_k(\mathbf{p}_j)) + wu (\pi_k(\mathbf{p}_i) + \pi_i(\mathbf{p}_k))\end{aligned}$$

Refinamento Adaptativo

$$d_i = \left(1 - \left\| \mathbf{n}_i^\top \frac{\mathbf{c} - \mathbf{p}_i}{\|\mathbf{c} - \mathbf{p}_i\|} \right\| \right) m$$

Comparações

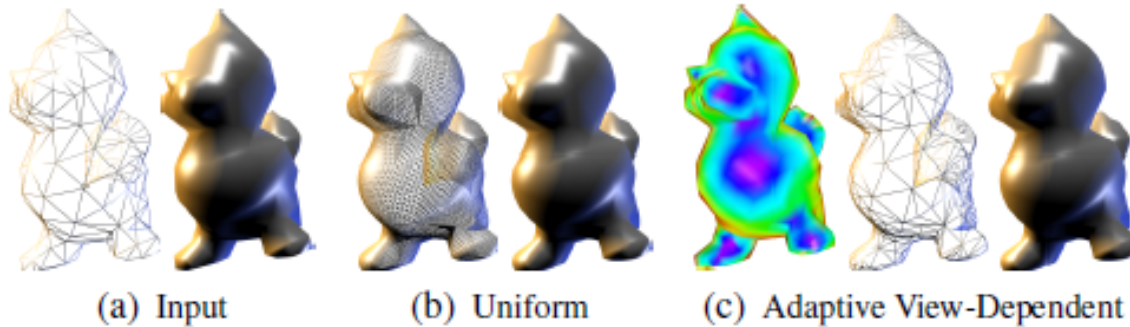


Figure 7: Adaptive view-dependent Phong Tessellation for real-time geometric upsampling on silhouettes and contours only.

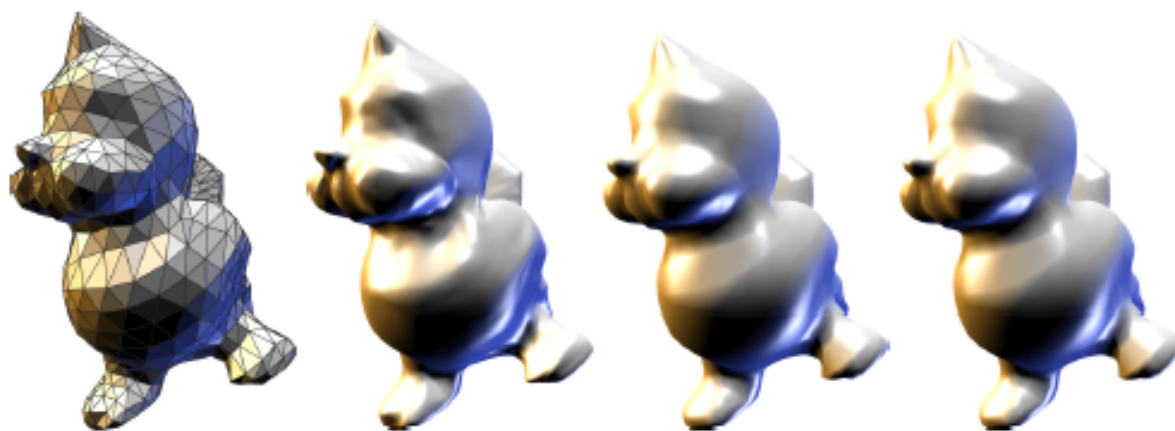


Figure 9: Comparison: Modified Butterfly subdivision (middle-left), PN Triangles (middle-right) and Phong tessellation (right).

ARTIGO 2:

Efficient GPU Rendering of Subdivision Surfaces using Adaptive Quadtrees

Wade Brainerd*
Activision

Tim Foley*
NVIDIA

Manuel Kraemer
NVIDIA

Henry Moreton
NVIDIA

Matthias Nießner
Stanford University

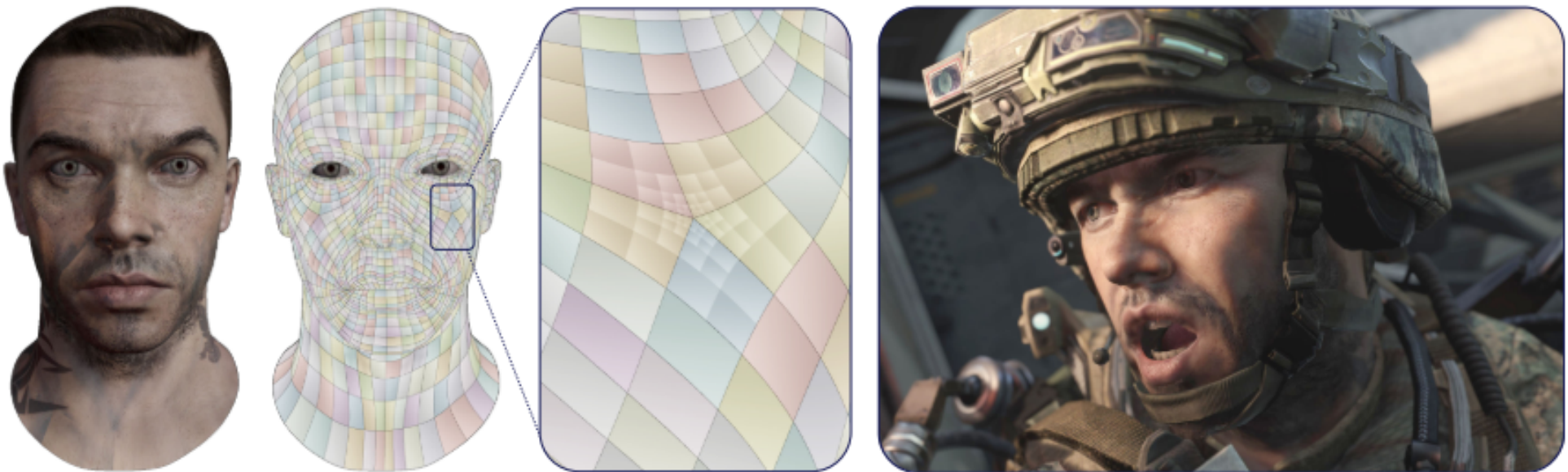
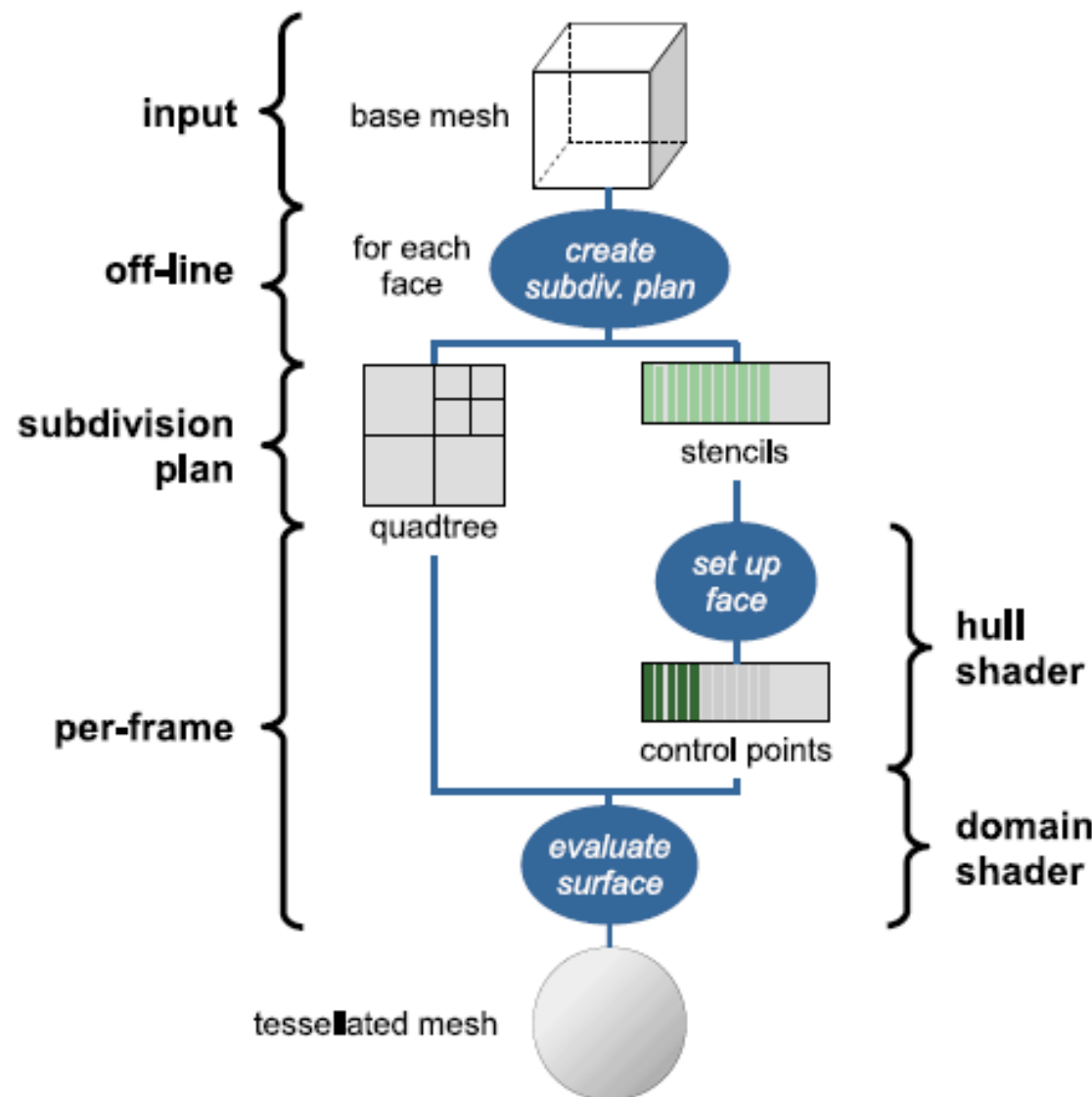


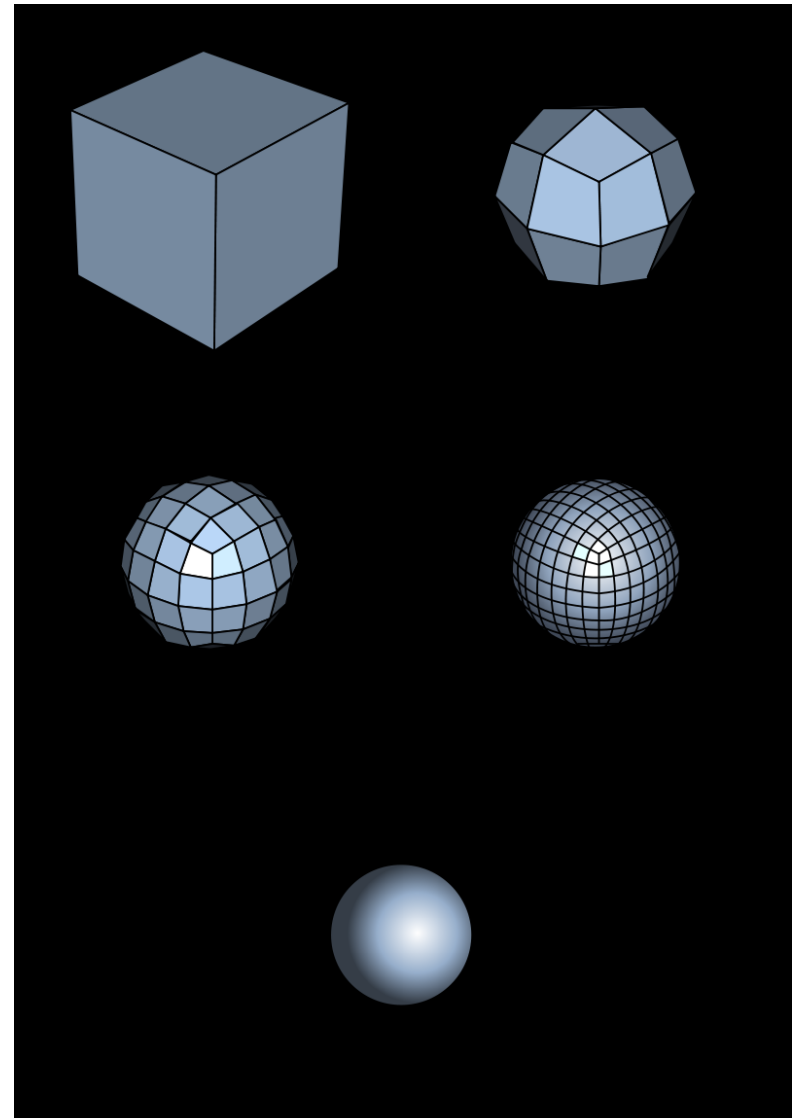
Figure 1: In our method, a subdivision surface model (left) is rendered in a single pass, without a separate subdivision step. Each quad face is submitted as a single tessellated primitive; a per-face adaptive quadtree is used to map tessellated vertices to the appropriate subdivided face (middle). Our approach makes tessellated subdivision surfaces easy to integrate into modern video game rendering (right). © 2014 Activision Publishing, Inc.

Visão Geral



Entrada de dados

- Catmull-Clark base mesh
 - Topologia
 - Tags de características
 - Vértices
- Atualizações dinâmicas de topologia



Plano de Subdivisão

- Uma estrutura de dados que representa uma hierarquia de subdivisões para uma face até um nível de detalhe máximo definido.
 - Uma *quadtree* das subdivisões hierárquicas de cada face
 - Uma lista ordenada de *Stencils*.
 - Cada *Stencil* representa uma soma balanceada dos vértices das faces na vizinhança “1-ring” do vértice

Plano de Subdivisão

- Catmull-Clark base mesh
 - Topologia
 - Tags de características
 - Vértices
- Atualizações dinâmicas de topologia

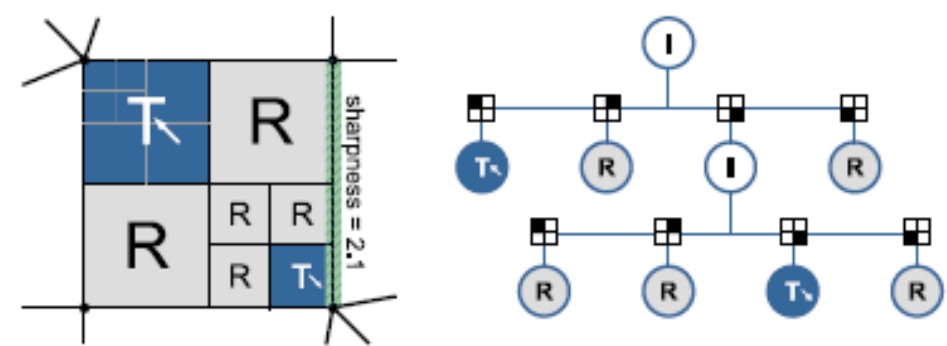


Figure 5: Quadtree for a face with two extraordinary vertices, and one semi-sharp edge. The quadtree comprises internal (I), regular (R), and terminal nodes (T). Our terminal nodes do not support direct semi-sharp crease evaluation, so the bottom-right quadrant is recursively subdivided until the sharp feature is eliminated.

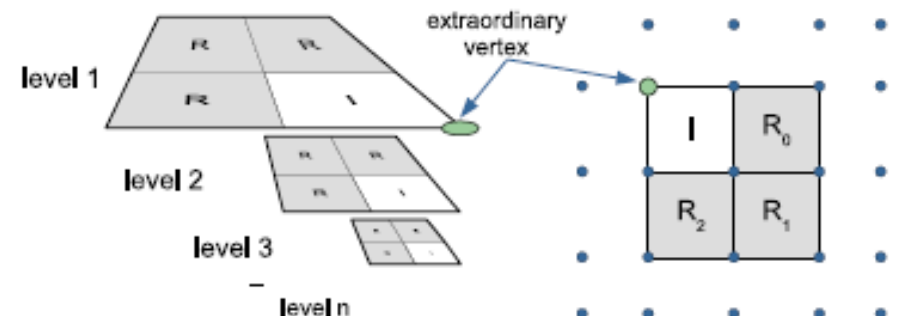
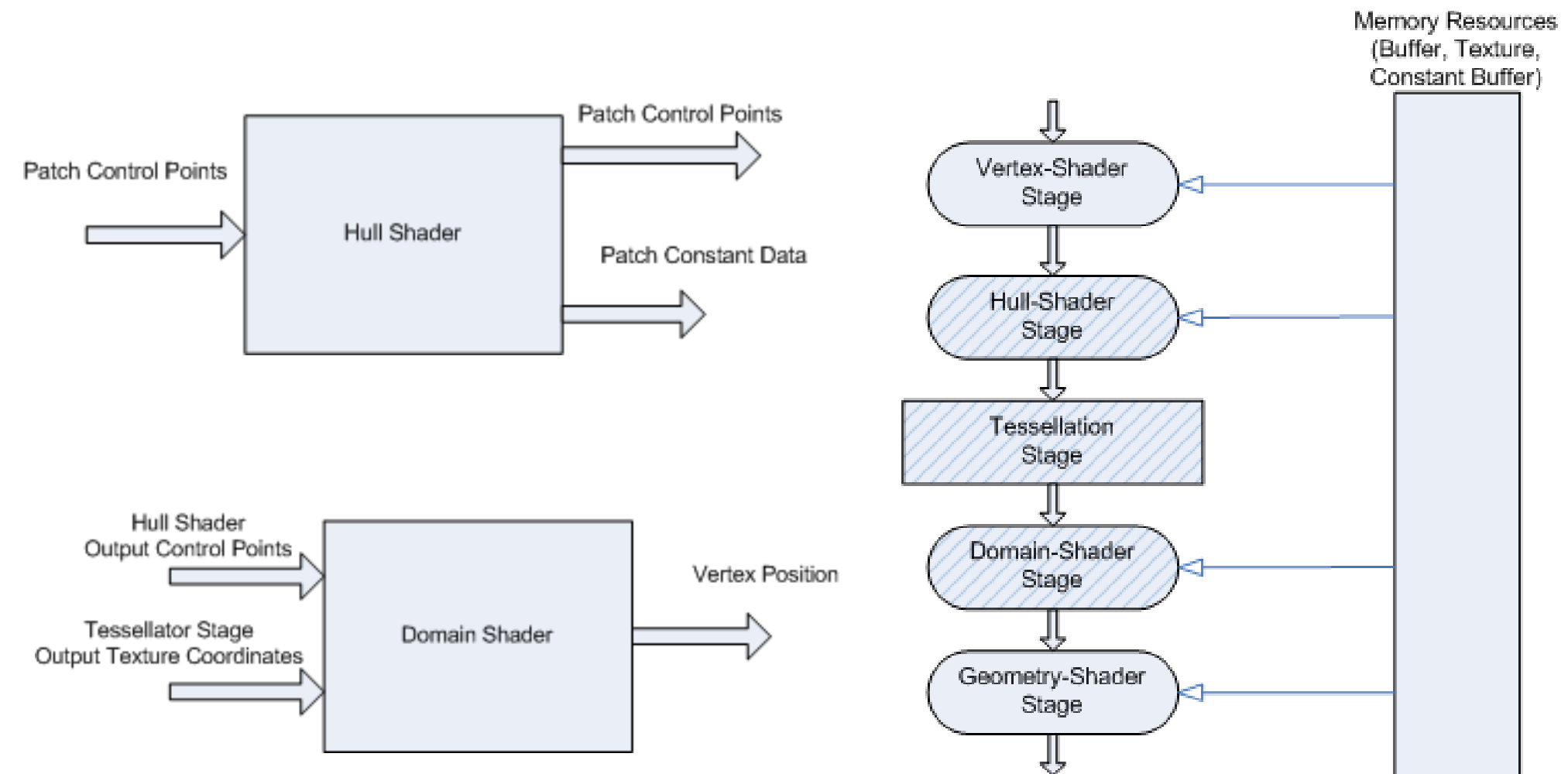


Figure 6: A terminal node captures the repeating pattern of adaptive subdivision at an extraordinary vertex (left). For each subdivision level, the node references 24 control points shared by three regular sub-domains (right).

Face Setup - Subdivision



Vértice extraordinário

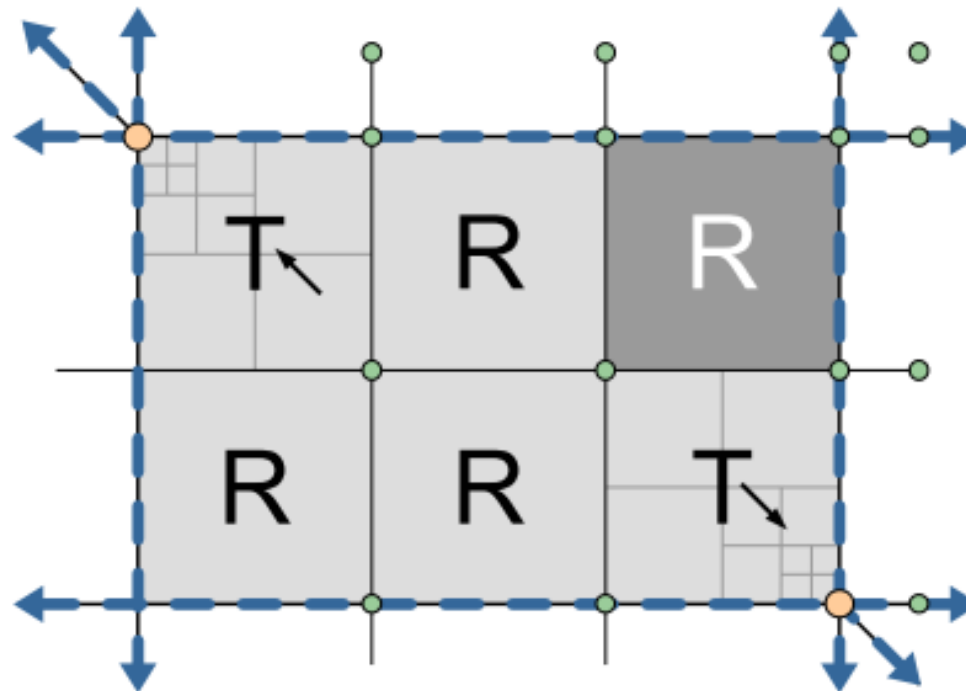


Figure 7: A 3×2 rectangular macro face formed by the intersections of separatrices from two extraordinary vertices (orange). Aggregated irregular faces (T) reference quadtree root nodes, while regular faces (R) share a grid of B-spline control points; the control points (green) used by the shaded regular face are shown.

Quadriláteros regulares e Irregulares

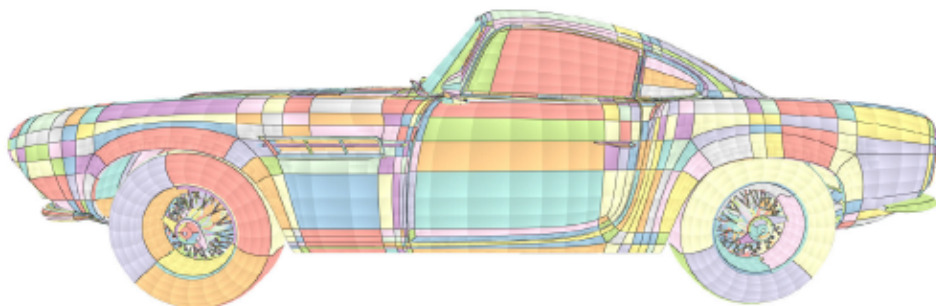


Figure 8: The Stirling model (©Disney/Pixar) rendered with rectangular macro faces. Colors indicate different macro faces; shading shows the parameter (sub-)domains of aggregated face quadtrees. The wheels show that macro face dimensions are limited to 16, allowing a maximum per-face tessellation factor of 4.

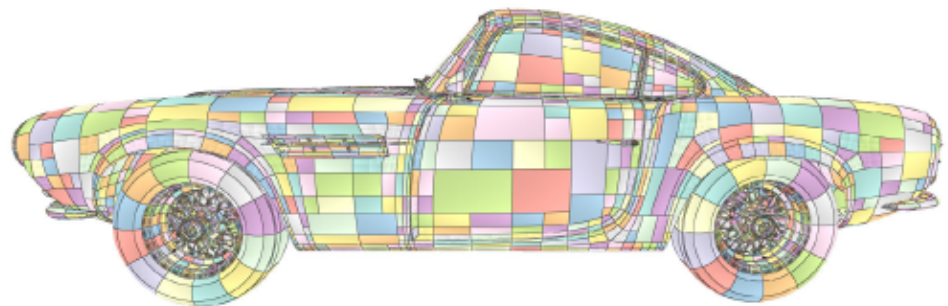


Figure 10: The Stirling model (©Disney/Pixar) with regular, quartet, and irregular faces. As the tessellation factor is uniform, quartets are allowed to be offset relative to one another.

8.1 Subdivision Ring Buffer

Comparações

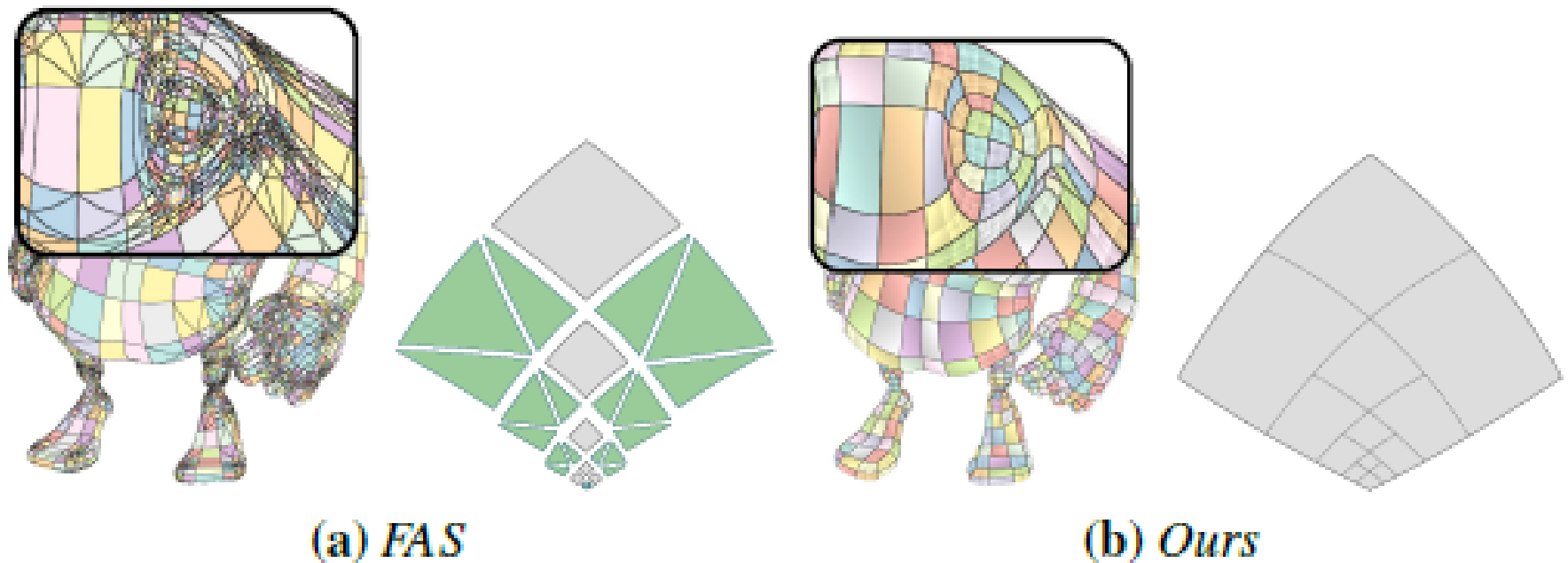


Figure 2: In order to isolate an extraordinary vertex, FAS subdivides a face into multiple primitives, including transition patches (green) to stitch T-junctions. Our algorithm uses a single primitive per quad face, with a precomputed internal hierarchy.

Comparações

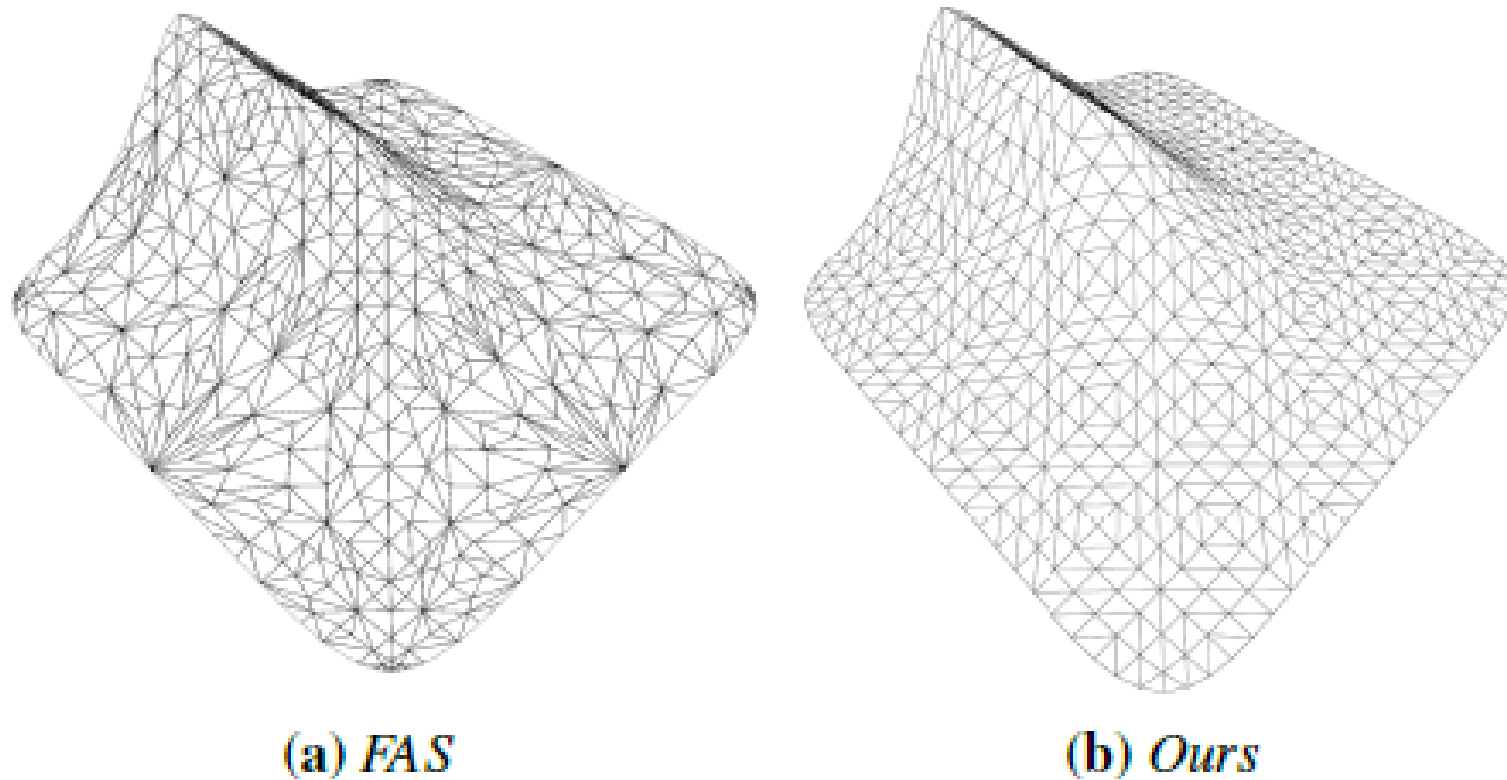


Figure 3: Comparison of tessellation pattern quality between FAS and our approach. Our tessellation density is more uniform due to our one-to-one mapping between submitted and rendered faces.

Comparações

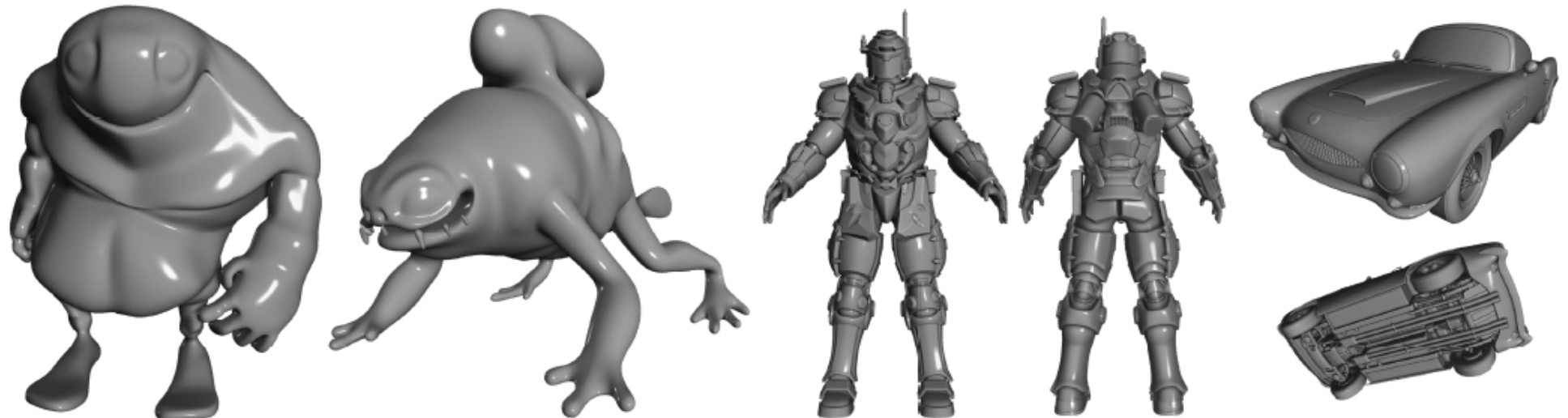
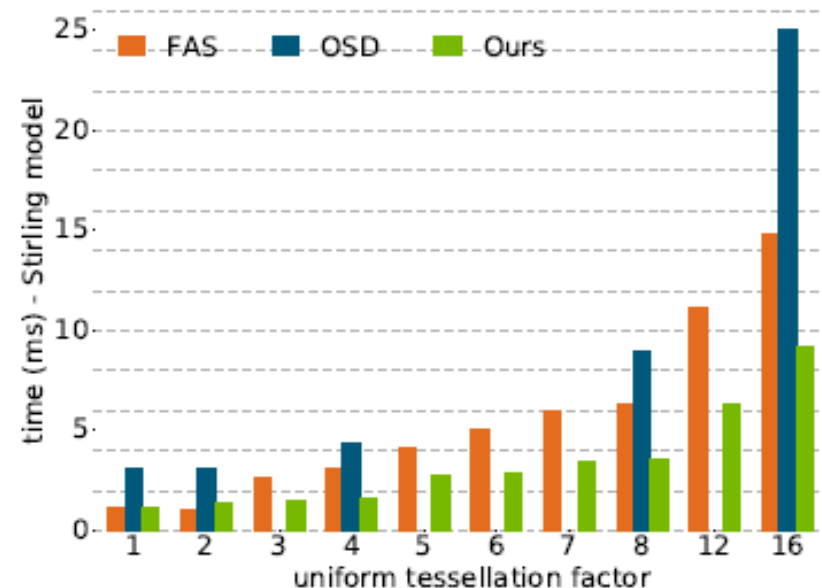
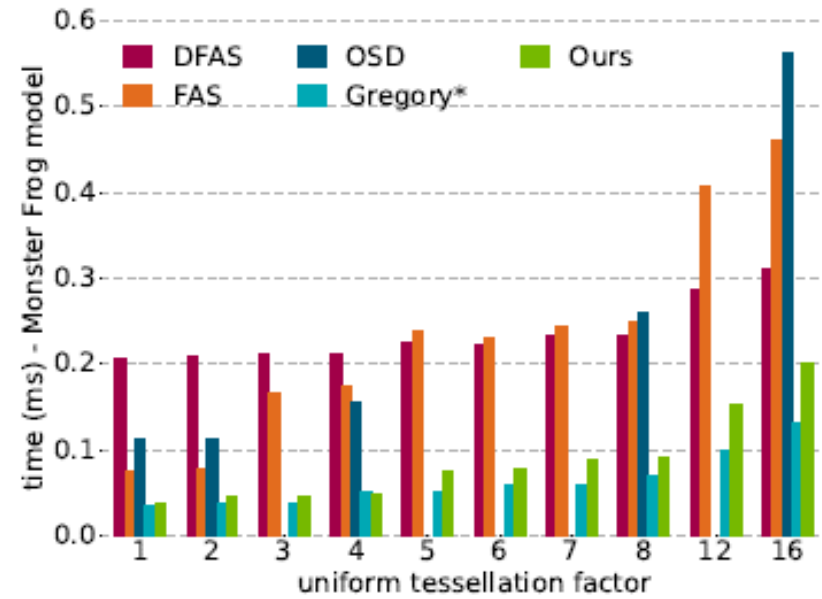
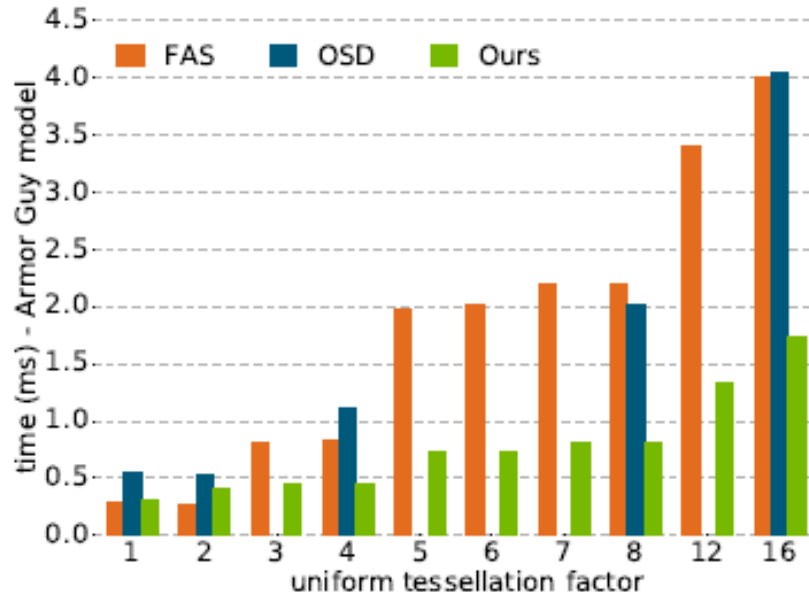
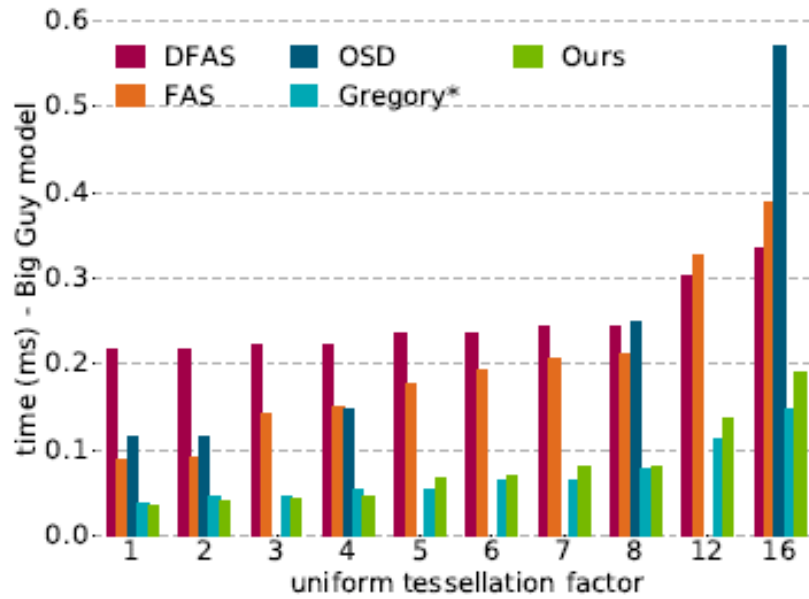


Figure 12: Models used in our evaluation, from left to right: *Big Guy*, *Monster Frog*, *Armor Guy* (©2014 DigitalFish, Inc. All rights reserved), and *Stirling* (©Disney/Pixar).

Comparações



Limitações

- Número fixo de profundidade máxima
- Número de vértices que o vertex shader pode passar para o hull shader (32 na implementação estudada).
- Funciona apenas com o modelo de subdivisão de Catmull-Clark

Artigo 3:

EUROGRAPHICS 2017/ A. Peytavie and C. Bosch

Short Paper

Phong Tessellation and PN Polygons for Polygonal Models

G.J. Hettinga¹, J. Kosinka¹

¹Johann Bernoulli Institute, University of Groningen, Nijenborgh 9, 9747 AG Groningen, The Netherlands

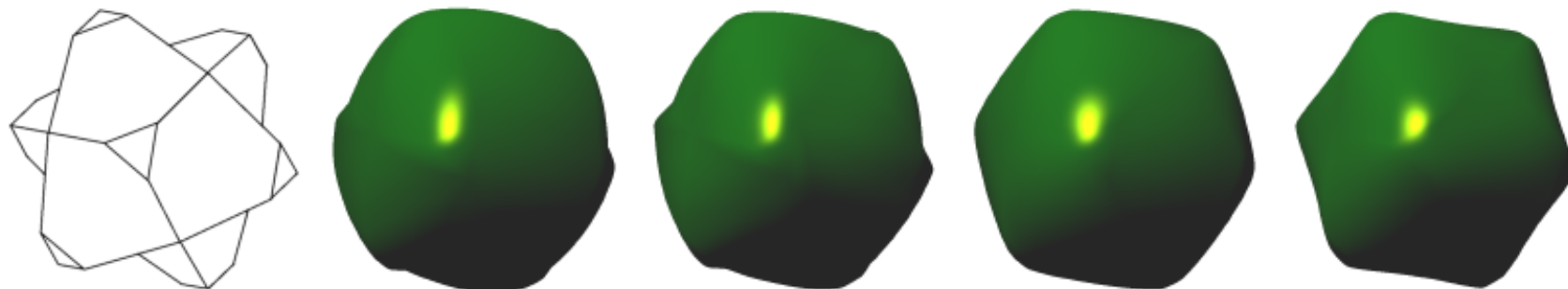


Figure 1: Rendering a model with 8 triangles and 12 non-planar hexagons. Left to right: input model, original Phong tessellation [BA08], original PN triangles [VPBM01] (hexagons have been triangulated), extended Phong tessellation, and PN triangles extended to PN polygons.

Generalização das coordenadas baricêntricas

Para um polígono qualquer:

- Partição da unidade
- Não negativos
- Reprodução linear

Existem várias formulações para se generalizar coordenadas baricêntricas.

Tesselagem linear e quadrática

$$\mathbf{p}(u, v, w) = (u, v, w)(\mathbf{v}_1, \mathbf{v}_2, \mathbf{v}_3)^T, \quad (1)$$

$$\mathbf{p}^2(u, v, w) = (u, v, w) \begin{pmatrix} \pi_1(\mathbf{p}(u, v, w)) \\ \pi_2(\mathbf{p}(u, v, w)) \\ \pi_3(\mathbf{p}(u, v, w)) \end{pmatrix}. \quad (2)$$

Tesselagem cúbica

$$\mathbf{p}^3(u, v, w) = \sum_{\substack{i+j+k=3 \\ i, j, k \geq 0}} \frac{3!}{i!j!k!} \mathbf{b}_{ijk} u^i v^j w^k, \quad (3)$$

where

$$\begin{aligned} \mathbf{b}_{300} &= \mathbf{v}_1, \quad \mathbf{b}_{030} = \mathbf{v}_2, \quad \mathbf{b}_{003} = \mathbf{v}_3, \\ \mathbf{b}_{210} &= \frac{2}{3}\mathbf{v}_1 + \frac{1}{3}\pi_1(\mathbf{v}_2), \quad \mathbf{b}_{120} = \frac{2}{3}\mathbf{v}_2 + \frac{1}{3}\pi_2(\mathbf{v}_1), \\ \mathbf{b}_{201} &= \frac{2}{3}\mathbf{v}_1 + \frac{1}{3}\pi_1(\mathbf{v}_3), \quad \mathbf{b}_{102} = \frac{2}{3}\mathbf{v}_3 + \frac{1}{3}\pi_3(\mathbf{v}_1), \\ \mathbf{b}_{021} &= \frac{2}{3}\mathbf{v}_2 + \frac{1}{3}\pi_2(\mathbf{v}_3), \quad \mathbf{b}_{012} = \frac{2}{3}\mathbf{v}_3 + \frac{1}{3}\pi_3(\mathbf{v}_2), \\ \mathbf{e} &= (\mathbf{b}_{210} + \mathbf{b}_{120} + \mathbf{b}_{201} + \mathbf{b}_{102} + \mathbf{b}_{021} + \mathbf{b}_{012})/6, \\ \mathbf{c} &= (\mathbf{v}_1 + \mathbf{v}_2 + \mathbf{v}_3)/3, \text{ and } \mathbf{b}_{111} = \mathbf{e} + (\mathbf{e} - \mathbf{c})/2. \end{aligned}$$

Extended Phong Tesselation

$$\mathbf{p}^2(\phi) = (\phi_1, \phi_2, \dots, \phi_n) (\pi_1(\mathbf{p}(\phi)), \dots, \pi_n(\mathbf{p}(\phi)))^\top. \quad (6)$$

Subdivisão cúbica representada em combinação
de subdivisões quadráticas

$$\mathbf{p}^3(u, v, w) = (u, v, w) \begin{pmatrix} (u, v, w) & \begin{pmatrix} \pi_1(\mathbf{p}(u, v, w)) \\ \mathbf{p}(u, v, w) \\ \mathbf{p}(u, v, w) \\ \mathbf{p}(u, v, w) \end{pmatrix} \\ (u, v, w) & \begin{pmatrix} \pi_2(\mathbf{p}(u, v, w)) \\ \mathbf{p}(u, v, w) \\ \mathbf{p}(u, v, w) \\ \mathbf{p}(u, v, w) \end{pmatrix} \\ (u, v, w) & \begin{pmatrix} \pi_3(\mathbf{p}(u, v, w)) \\ \mathbf{p}(u, v, w) \\ \mathbf{p}(u, v, w) \\ \mathbf{p}(u, v, w) \end{pmatrix} \end{pmatrix} + \boldsymbol{\theta}_3$$

with

$$\boldsymbol{\theta}_3 = 6uvw \left(\frac{-\mathbf{c}_{123} + \sum_{q \in \{1,2,3\}} \pi_q(\mathbf{c}_{123})}{4} \right),$$

Interpolação de normais

$$\tau_i(\mathbf{n}, \mathbf{v}) = \begin{cases} \mathbf{n}, & \text{if } \mathbf{v} = \mathbf{v}_i \\ \mathbf{n} - 2 \frac{\mathbf{n} \cdot (\mathbf{v} - \mathbf{v}_i)}{(\mathbf{v} - \mathbf{v}_i) \cdot (\mathbf{v} - \mathbf{v}_i)} (\mathbf{v} - \mathbf{v}_i), & \text{otherwise,} \end{cases}$$

$$\mathbf{n}^2(\boldsymbol{\phi}) = \boldsymbol{\phi} \left(\boldsymbol{\phi} \begin{pmatrix} \tau_1(\mathbf{n}_1, \mathbf{v}_1) \\ \dots \\ \tau_1(\mathbf{n}_n, \mathbf{v}_n) \end{pmatrix}, \dots, \boldsymbol{\phi} \begin{pmatrix} \tau_n(\mathbf{n}_1, \mathbf{v}_1) \\ \dots \\ \tau_n(\mathbf{n}_n, \mathbf{v}_n) \end{pmatrix} \right)^T. \quad (10)$$

Resultados



Figure 2: Reflection lines on a cubic triangle for various normal interpolation methods. Left to right: linear interpolation, quadratic interpolation for PN triangles, and the new quadratic interpolation for arbitrary PN polygons.

Resultados

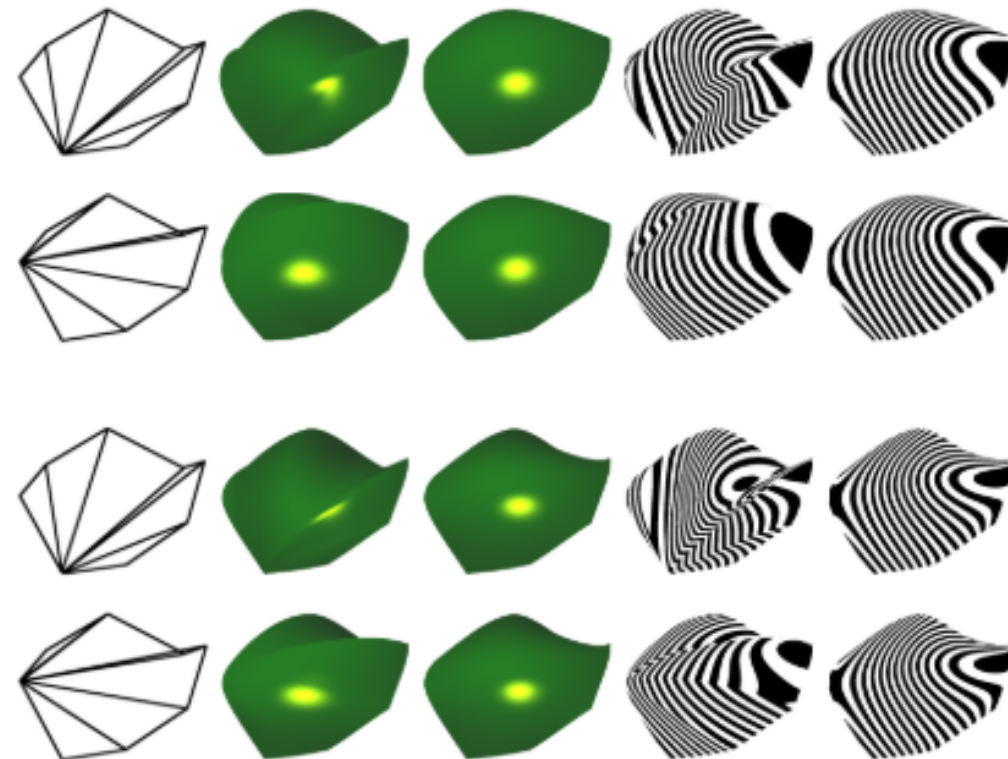


Figure 3: Comparison: Two different triangulations of a non-planar octagon. Top two rows: Phong tessellation and extended Phong tessellation, reflection lines of linear normal fields on Phong tessellation and extended Phong tessellation. Bottom two rows: PN triangles and PN polygons, reflection lines of the new quadratic normal fields, see (10), on PN triangles and PN polygons. Note that extended Phong tessellation and PN polygons are independent of the triangulation of the input octagon.

Desempenho

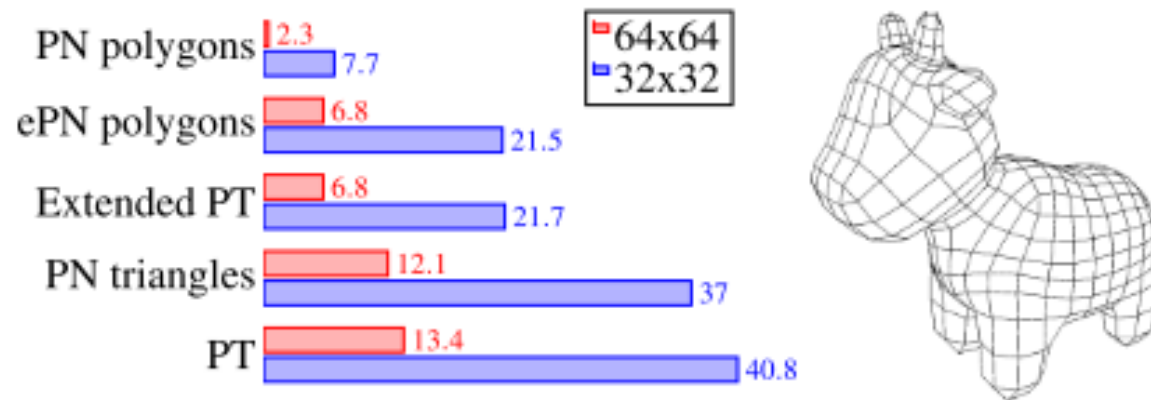


Figure 4: Performance comparison in FPS per method: rendering a model (right) containing 56 triangles, 634 quads, 40 pentagons, and 4 hexagons at two tessellation depths. ePN polygons refers to the explicit calculation of control points, see (9), and PT refers to Phong tessellation.

Conclusão

Apesar do desempenho mais lento em relação as soluções comparadas, as extensões propostas no artigo conseguem criar superfícies complexas independente da triangulação do polígono